Cooperative cluster Jahn-Teller effect as a possible route to antiferroelectricity

Korbinian Geirhos, Jan Langmann, Lilian Prodan, Alexander A. Tsirlin, A. Missiul, Georg Eickerling, Anton Jesche, Vladimir Tsurkan, Peter Lunkenheimer, Wolfgang Scherer, István Kézsmárki

Angaben zur Veröffentlichung / Publication details:

Geirhos, Korbinian, Jan Langmann, Lilian Prodan, Alexander A. Tsirlin, A. Missiul, Georg Eickerling, Anton Jesche, et al. 2021. "Cooperative cluster Jahn-Teller effect as a possible route to antiferroelectricity." *Physical Review Letters* 126 (18): 187601. https://doi.org/10.1103/physrevlett.126.187601.

Cooperative Cluster Jahn-Teller Effect as a Possible Route to Antiferroelectricity

K. Geirhos,[1] J. Langmann,[2] L. Prodan,[1,3] A. A. Tsirlin,[4] A. Missiul,[5] G. Eickerling,[2] A. Jesche,[4] V. Tsurkan,[1,3] P. Lunkenheimer,[1] W. Scherer,[2] and I. Kézsmárki[1]

[1]*Experimental Physics V, Center for Electronic Correlations and Magnetism, University of Augsburg, 86135 Augsburg, Germany*

[2]*CPM, Institute of Physics, University of Augsburg, 86135 Augsburg, Germany*

[3]*Institute of Applied Physics, MD 2028, Chisinau, Republic of Moldova*

[4]*Experimental Physics VI, Center for Electronic Correlations and Magnetism, University of Augsburg, 86135 Augsburg, Germany*

[5]*CELLS-ALBA Synchrotron, Cerdanyola del Valles, E-08290 Barcelona, Spain*

(Received 16 September 2020; revised 2 March 2021; accepted 8 April 2021; published 4 May 2021)

We report the observation of an antipolar phase in cubic $GaNb_4S_8$ driven by an unconventional microscopic mechanism, the cooperative Jahn-Teller effect of Nb_4S_4 molecular clusters. The assignment of the antipolar nature is based on sudden changes in the crystal structure and a strong drop of the dielectric constant at $T_{JT} = 31$ K, also indicating the first-order nature of the transition. In addition, we found that local symmetry lowering precedes long-range orbital ordering, implying the presence of a dynamic Jahn-Teller effect in the cubic phase above T_{JT}. Based on the variety of structural polymorphs reported in lacunar spinels, also including ferroelectric phases, we argue that $GaNb_4S_8$ may be transformable to a ferroelectric state, which would further classify the observed antipolar phase as antiferroelectric.

DOI: 10.1103/PhysRevLett.126.187601

Macroscopic stray fields inherent to ferromagnetic and ferroelectric orders allow coupling to uniform external fields and make these states easy to identify and control. Therefore, ferromagnetic and ferroelectric materials are extensively used in various applications, most prominently in information technology. In contrast, in antiferromagnetic and antiferroelectric (AFE) materials no macroscopic stray fields develop due to the staggered order of dipoles. Until the development of neutron diffraction, this hindered the direct observation of antiferroic ordering [1]. However, when it comes to memory applications, the absence of stray fields can be an advantage, leading to the robustness of antiferroic states against unwanted switchings by disturbing macroscopic fields. The great potential of antiferromagnets in information technology has triggered an enormous progress in antiferromagnetic spintronics, a recently emerging field of magnetism [2–5].

Though AFE compounds are also of fundamental interest and can possess similar advantages as their magnetic counterparts, this type of order is much less explored due to conceptual difficulties in defining the basic criteria of antiferroelectricity and identifying its unique experimental signatures. Besides studies on model-type perovskite antiferroelectrics [6–10] and antiferroelectricity in liquid crystals [11], there are only few reports on AFE order in other material classes [12–18].

Current approaches define antiferroelectricity via its onset: Accordingly, AFE transitions represent a class of symmetry-lowering structural transitions between two nonpolar phases, upon which some of the crystallographic sites become polar [10,19,20]. As an experimental feature, the transition to the AFE state is associated with a drop of the dielectric constant [10]. In terms of symmetry, the onset of antiferroelectricity requires the point group of a symmorphic subgroup of the lower-symmetry (AFE) space group to coincide with the site symmetry of at least one of the sites that become polar upon the transition [20]. In addition, an alternative polar distortion of the nonpolar high-symmetry phase into a ferroelectric phase is required to render the antipolar phase also antiferroelectric [19]. If this ferroelectric state and the AFE state are separated by a sufficiently low-energy barrier, a transition between them can be driven by laboratory electric fields.

Here, we investigate the emergence of antiferroelectricity in the AM_4X_8 lacunar spinel family, a class of cluster Mott insulators [21–23]. The lacunar spinel structure can be derived from the normal spinel structure AM_2X_4 by removing every second A-site ion, resulting in a noncentrosymmetric cubic structure with the space group $F\bar{4}3m$. These materials are often considered as molecular crystals with weakly linked M_4X_4 and AX_4 clusters, as seen in Fig. 1(a) [24–27]. The electronic configuration of the M_4X_4 cubane clusters, within a molecular orbital scheme, leads to an unpaired electron in GaV_4X_8 and $GaNb_4X_8$ and an unpaired hole in $GaMo_4X_8$, occupying a triply degenerate molecular orbital, with X being S or Se [see Fig. 1(b)] [28]. This makes the M_4X_4 molecular cluster magnetic and Jahn-Teller active.

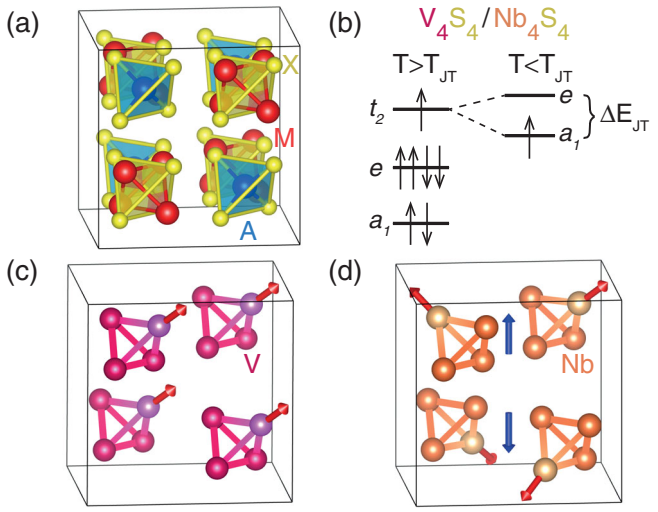

FIG. 1. (a) Structural model of the cubic lacunar spinels AM_4X_8. (b) Molecular orbital scheme and electronic configuration of M_4X_4 clusters for M = Nb, V, and X = S in the cubic and the low-temperature distorted phase without considering spin-orbit effects. (c),(d) Main motif of the Jahn-Teller distortion of the M_4 tetrahedra for GaV_4S_8 and $GaNb_4S_8$, respectively. Red arrows indicate the main distortion component for individual M_4 units, while blue arrows indicate the sum of the distortions for the upper and lower Nb_4 units.

The orbital degeneracy of the cubic phase, accordingly, is lifted by a cooperative Jahn-Teller distortion of the M_4X_4 units. In case of GaV_4S_8, GaV_4Se_8, and $GaMo_4S_8$ the ferrodistortive nature of the transition leads to a polar state, making these materials rare examples of orbital-order driven ferroelectrics [29–34]. For GaV_4S_8 it was even found that the ferroelectric transition is of order-disorder type, meaning that the cooperative Jahn-Teller distortion below T_{JT} is preceded by a dynamic Jahn-Teller effect [35]. Upon the nonpolar to polar transition, taking place between 40 and 50 K depending on the material, all M_4X_4 clusters get distorted along the same cubic body diagonal, reducing the symmetry to rhombohedral (space group $R3m$) [28–31], as seen in Fig. 1(c). The point group of the crystal coincides with that of the rhombohedrally distorted M_4X_4 cubanes ($3m$). Recently, electric and magnetic control of ferroelectric domains [30,31,36,37], magnetoelectric effects [36,38], and skyrmion lattices [39–42] have been reported in these compounds.

In contrast, in $GaNb_4S_8$ the orbital degeneracy of the Nb_4S_4 units is lifted by a more complex distortion, which leads to a stronger symmetry reduction of the Nb_4S_4 units to point group m [43]. Still, similar to its ferrodistortive sister compounds, the main motif in the Jahn-Teller driven deformation of individual Nb_4S_4 clusters is the rhombohedral distortion, i.e., an elongation parallel to one of the cubic body diagonals, inducing polar moments on the Nb_4S_4 units. However, the cooperative distortion of four adjacent Nb_4S_4 units below T_{JT} is along four different cubic body diagonals, as sketched in Fig. 1(d), thus preventing the development of a macroscopic polarization and leading to an overall tetragonal symmetry [43]. Interestingly, this tetragonal distortion in $GaNb_4S_8$ from space group $F\bar{4}3m$ to space group $P\bar{4}2_1m$ fulfills the group-theoretical criterion for AFE transitions [10,20]: Ga is the only atom occupying a Wyckoff position with nonpolar site symmetry $\bar{4}3m$ in the cubic phase. Upon the transition to the tetragonal phase, a polar site symmetry m is obtained for Ga that coincides with the point group of the symmorphic subgroups $C1m1$ and $P1m1$ of $P\bar{4}2_1m$. A symmetry-mode decomposition analysis of the structural transition also revealed that the distortion is dominated by the Jahn-Teller active X_5 mode that lifts the orbital degeneracy of the Nb_4 units (see Table S2 in the Supplemental Material [44], including Refs. [29–31,43,45–61]).

To further investigate the nature of the Jahn-Teller transition and the possible emergence of antiferroelectricity in $GaNb_4S_8$, we apply a multiprobe approach, including dielectric spectroscopy, single-crystal and high-resolution powder x-ray diffraction (XRD), specific heat, magnetic susceptibility measurements. Our results evidence that the orbital degeneracy of Nb_4S_4 clusters drives a first-order transition to a nonmagnetic antipolar phase at $T_{JT} = 31$ K. The powder XRD measurements, in addition, also suggest the presence of a dynamic Jahn-Teller effect in the cubic phase above T_{JT}.

All experiments, except the powder XRD, were performed on single crystals grown by the chemical transport reaction method. (For experimental details, see the Supplemental Material [44]).

Figures 2(a) and 2(c) display reconstructions of the $(hk0)$ reciprocal-space plane from single-crystal XRD experiments at 42 and 14 K, respectively. (For extended and additional reciprocal-space planes, see Fig. S2 [44].) Below $T_{JT} = 31$ K, diffracted intensity was detected at positions of previously forbidden reflections of the type $hkl: h + k, h + l, k + l = 2n + 1$ [see Figs. 2(b) and 2(d)]. This is compatible with the symmetry lowering from the cubic space group $F\bar{4}3m$ [$a = 9.9837(2)$ Å] to the tetragonal space group $P\bar{4}2_1m$ reported earlier [43]. Interestingly, we found additional weak reflections at half-integer positions indicating a doubling of one unit-cell axis [Fig. 2(d)].

To detect potential small changes in the cell metrics, we performed synchrotron powder XRD experiments at ALBA. As shown in Fig. 2(e), below T_{JT} the $(4, 0, 0)$ reflection splits into three peaks with nearly equal intensities, indicating that the symmetry of the low-temperature phase is not higher than orthorhombic. [The tetragonal $P\bar{4}2_1m$ symmetry would lead to a splitting of $(4, 0, 0)$ into two peaks.] Both single-crystal and powder XRD data are consistent with a description of the low-temperature structure in the nonpolar but chiral orthorhombic space group $P2_12_12_1$ [$a = 9.9873(4)$, $b = 9.9749(3)$, $c = 19.9775(6)$ Å]. (For a comparison of the crystallographic data above and below T_{JT}, see Table S1 [44].) This space group choice

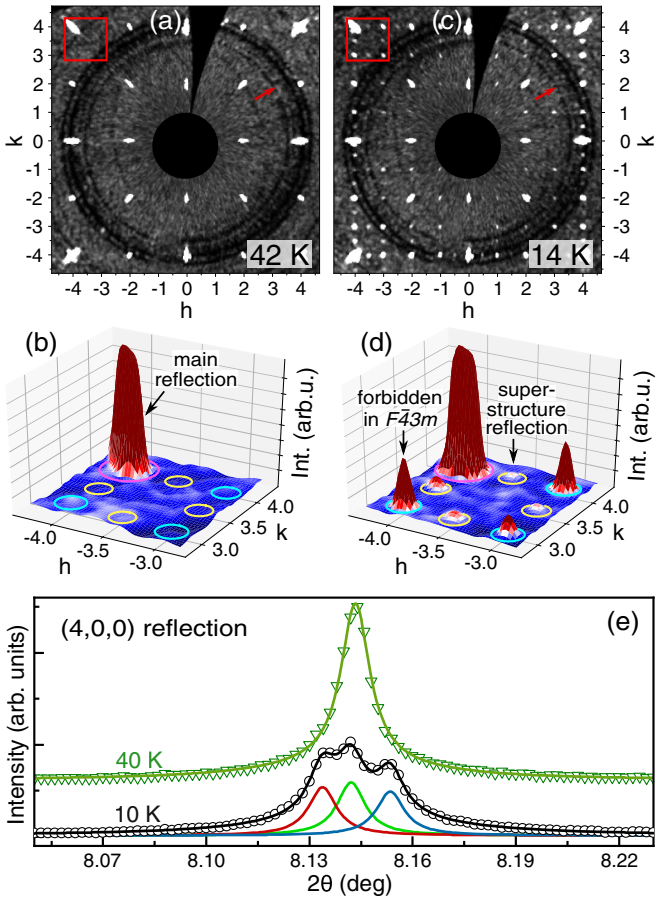

FIG. 2. Reconstructions of the $(hk0)$ reciprocal-space plane measured at (a) 42 and (c) 14 K. An overview of the different reflection types visible at 42 and 14 K is given by three-dimensional plots (b),(d) of the regions marked by red rectangles in (a) and (c). Intense main reflections in (b) and (d) are clipped. Ring-shaped features marked by red arrows are due to parasitic scattering. (e) The fine structure of the $(4, 0, 0)$ reflection measured by powder XRD at 40 and 10 K. The solid black and dark green lines represent fits of the data. A decomposition of the threefold-split reflection at 10 K is indicated by solid red, green, and blue lines.

takes into account the orthorhombicity, the extinction condition $h00, h = 2n$, $0k0, k = 2n$, and $00l, l = 2n$, and a unit-cell doubling along the c axis. Very low intensities of the superstructure reflections, unfortunately, do not allow the extraction of the detailed distortion pattern. However, the low intensities also suggest that the distortion should be dominated by the same X_5 mode as for the $P\bar{4}2_1m$ model and thus reflect the Jahn-Teller instability. Still, it is clear that the remaining mirror-plane symmetry of the Nb_4 clusters in space group $P\bar{4}2_1m$ is lost in space group $P2_12_12_1$. Correspondingly, the site symmetry of Ga, Nb, and S is reduced to polar 1 coinciding with the point group of the symmorphic polar subgroup $P1$ of $P2_12_12_1$. Therefore, the transition from $F\bar{4}3m$ to $P2_12_12_1$ also fulfills the symmetry criterion for AFE transitions [20].

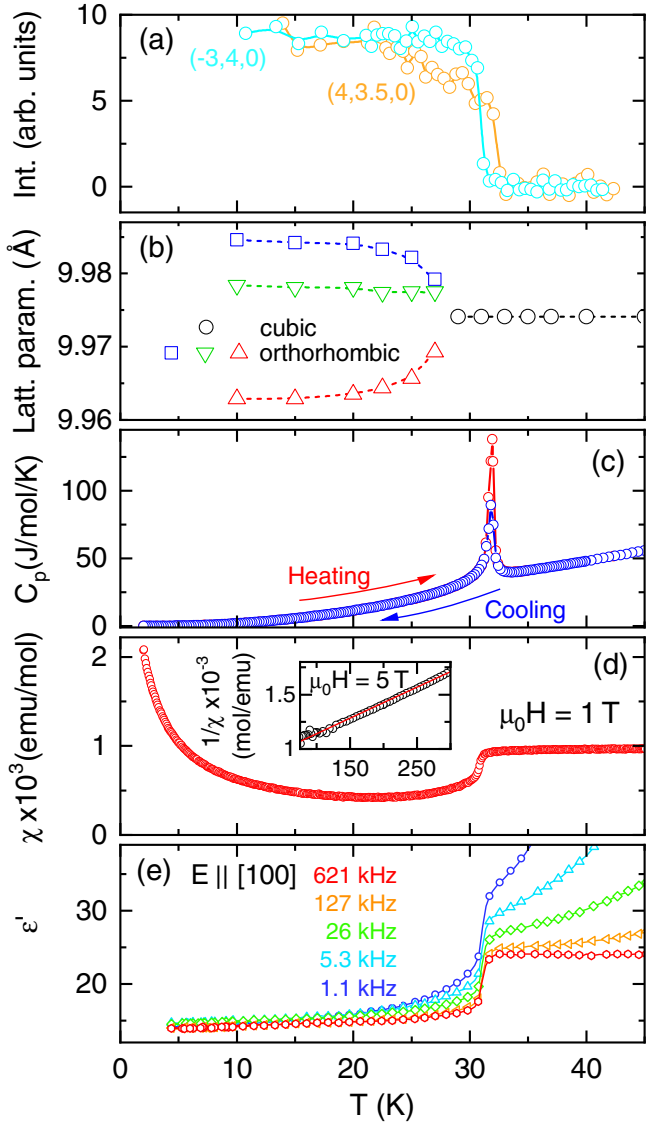

FIG. 3. Temperature dependence of (a) the reflection intensities at positions $(-3, 4, 0)$ and $(4, 3.5, 0)$ as recorded by single-crystal XRD (rescaled to the same intensity level at low temperatures), (b) the lattice parameters, (c) specific heat, (d) magnetic susceptibility, and (e) dielectric constant at different frequencies. The inset in (d) displays the inverse susceptibility at elevated temperatures.

To determine the temperature dependence of the structural distortion, we recorded the intensity of the $(-3, 4, 0)$ reflection, forbidden in the high-temperature space group, and the intensity of the $(4, 3.5, 0)$ reflection, indicating the cell doubling [Fig. 3(a)]. With decreasing temperature, a sudden appearance of intensity is observed at T_{JT}, followed by a weak gradual increase toward lower temperatures. This points to a first-order character of the transition. An abrupt change of the lattice parameters and the cell volume as determined by powder XRD measurements [Fig. 3(b) and Fig. S3 [44]] further supports the first-order nature. We also observe higher peak values of the λ-shaped anomaly of

specific heat on heating than on cooling [Fig. 3(c)], characteristic for first-order transitions, caused by the latent heat associated with the transition. In the lacunar spinels undergoing a ferroelastic-ferroelectric distortion, the transition was also found to be of weakly first order [29,30,32,54].

As a key result of this Letter, the temperature dependence of the dielectric constant in Fig. 3(e) reveals a discontinuous, ~30% decrease at T_{JT}. The structural transition, therefore, does not only fulfill the symmetry criterion for an AFE transition, but this instantaneous drop of the dielectric constant also agrees with the theoretical expectations for a first-order AFE transition [10,20]. Though the existence of and the possible switching to an alternative polar state will be discussed later, we tentatively refer to the antipolar state as an AFE state. The jump is seen at each frequency, though the intrinsic plateaulike behavior of ε' above T_{JT} is masked by a gradual increase observed for low frequencies due to extrinsic Maxwell-Wagner relaxation [62,63]. This behavior of ε' is distinct from that of the polar sister compounds, where ε' exhibits a peak at T_{JT}, characteristic of ferroelectric ordering [29,32,40]. $GaNb_4S_8$ is, therefore, the first material where the Jahn-Teller activity of molecular clusters has been identified as a potential driving mechanism of AFE ordering.

Remarkably, our powder XRD studies also reveal that local symmetry lowering precedes the cooperative Jahn-Teller transition, pointing to a dynamic Jahn-Teller effect in the cubic phase. This is evidenced by an anisotropic peak broadening. The broadening can be decomposed into isotropic and anisotropic contributions using the parameters LY and LYe, respectively. As can be seen in Fig. 4, the isotropic part LY does not change significantly upon cooling, whereas the anisotropic part LYe increases as the temperature approaches T_{JT} from higher temperatures. The observation of a dynamic Jahn-Teller effect is also in agreement with the enhanced structural fluctuations observed by nuclear magnetic resonance well above T_{JT} [64], which classifies this transition as an order-disorder type.

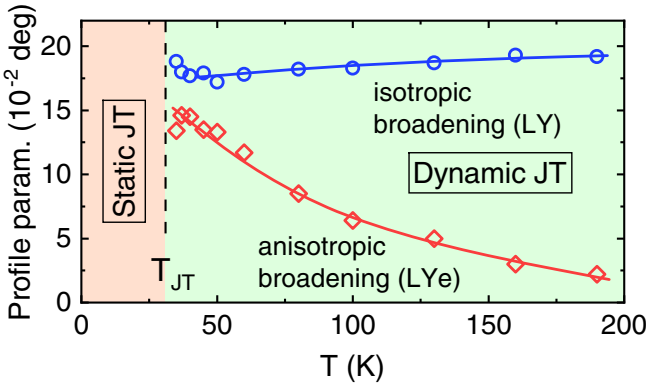

FIG. 4. Isotropic (LY) and anisotropic (LYe) contributions to the peak width by powder XRD above T_{JT}. The lines are guides to the eye.

The structural transition has a strong impact not only on the polar but also on the magnetic state of $GaNb_4S_8$. The sudden drop of the magnetic susceptibility at T_{JT}, shown in Fig. 3(d), implies that the first-order structural transition is accompanied by spin-singlet formation, as concluded from nuclear magnetic resonance studies [64]. The antiferromagnetic exchange is clearly manifested in the large, negative Curie-Weiss temperature of $\theta = -300$ K, as determined from the fit of the inverse susceptibility in the inset of Fig. 3(d) [27,43]. A similar interlocking between the structural transition and the onset of a nonmagnetic state has been recently observed in $GaNb_4Se_8$ and $GaTa_4Se_8$ [65]. In these compounds, the spin-orbit coupling, in interplay with the Jahn-Teller effect of the M_4Se_4 clusters, was identified as the driving force of the magnetostructural transition. While crystal-field effects usually dominate over spin-orbit coupling in semiconductors based on 3*d* transition metals, spin-orbit coupling has an increasing impact on the electronic structure of 4*d* and 5*d* compounds. Thus, spin-orbit coupling has to be taken into account for the proper description of the cluster orbitals in these compounds and the microscopic mechanism behind their magnetostructural transitions. In fact, in $GaNb_4Se_8$ and $GaTa_4Se_8$, the relevance of spin-orbit coupling is clearly manifested in the strong reduction of their effective paramagnetic moments from the $S = 1/2$ spin-only value. However, for $GaNb_4S_8$, we obtained an effective moment of $\mu_{eff} = 1.67\ \mu_B$/f.u. from susceptibility measurements, which is very close to the spin-only value (1.73 μ_B/f.u.). This implies the secondary role of spin-orbit physics and the dominance of the Jahn-Teller active Nb_4 cluster in driving the structural transition.

In addition, we observed a very weak polarization below T_{JT} [see Figs. S4 [44]]. Such a weak polarization superimposed on AFE order was previously observed in several materials and ascribed to different origins, like polar domain walls or tiny canting of the antipolar order [57–59]. Since a detailed analysis is beyond the scope of this Letter, a discussion of the weak polarization is provided in the Supplemental Material [44].

Unfortunately, we did not succeed with transforming the antipolar state to a polar state by electric fields. In this respect, the narrow gap (~0.2 eV) and the lower resistivity of the material, compared to other oxide antiferroelectrics [7,66,67], introduce strong limitations on the magnitude of static electric fields applicable. Nonresonant photo-induced switching via the strong electric field of intense terahertz radiation could be one approach to overcome this limitation. In the following, we argue that $GaNb_4S_8$ is a potential AFE material; i.e., it likely has a polar phase with energy close to that of the antipolar ground state. While lacunar spinels share a cubic structure at room temperature, they realize a variety of polymorphs below the structural transition. Prime examples are GaV_4S_8, $GaTa_4Se_8$, and $GaNb_4Se_8$ with a polar rhombohedral ($R3m$), antipolar

tetragonal ($P\bar{4}m2$), and chiral orthorhombic ($P2_12_12_1$) ground state, respectively [28,65]. $GaNb_4Se_8$ even has a chiral cubic phase ($P2_13$) at intermediate temperatures [65]. Despite this structural diversity, their common aspect is that the distortion of individual M_4X_4 units is well approximated by a rhombohedral distortion, as schematically shown in Fig. 1 for GaV_4S_8 and $GaNb_4S_8$. The primary role of the single-cluster distortion in the structural transformation is clear from the hierarchy of energy scales. The Jahn-Teller splitting (ΔE_{JT}) arising from the distortion of individual clusters is larger than the charge gap, since the corresponding electric-dipole excitation was not observed in the optical conductivity within the gap [22]. This implies the presence of a dynamic Jahn-Teller effect well above T_{JT}, as was indeed reported for GaV_4S_8 and is also evidenced for $GaNb_4S_8$ by our powder XRD measurements (see Fig. 4) [35,64].

Since the structural transition takes place at much lower temperatures ($k_BT_{JT} \sim 3$ meV $\ll \Delta E_{JT} \sim 300$ meV), the cooperative long-range ordering must be governed by weak interactions, such as intercluster interactions or strain. As T_{JT} varies between 30 and 50 K for all these compounds, the energy difference between the polymorphs, including the polar and the antipolar states, should be less than k_BT_{JT}. Thus, we believe that switching between the polymorphs via the proper conjugate fields should, in principle, be possible. Unfortunately, *ab initio* calculations may not be able to provide a realistic estimate for the energy difference between the antipolar and polar states of $GaNb_4S_8$. Because of the interplay of various factors (narrow gap, interplay between on-cluster correlations and spin-orbit effects, sensitivity of intercluster hopping to the orbital character of the single-cluster states), density-functional theory with the Hubbard U parameter schemes have not been able to reproduce the finite gap in the cubic state of the material (see [22] and references therein). Thus, to determine the energies of the polymorphs with a few meV precision is a great challenge for theory. These fundamental aspects of the correlated cluster-insulator $GaNb_4S_8$, distinguish this compound from $DyVO_4$, where the cooperative Jahn-Teller effect caused by Dy^{3+} ions was identified as the origin of AFE order.

In summary, we have performed structural, dielectric, specific heat, and magnetic studies to elucidate the polar and magnetic state of the lacunar spinel $GaNb_4S_8$ below its structural transition at $T_{JT} = 31$ K. Our combined single-crystal and powder XRD measurements revealed a unit-cell doubling along the c axis and a structural distortion compatible with space group $P2_12_12_1$ below T_{JT}. We demonstrate that the transition leads to the transformation of the nonpolar cubic state to an antipolar state, driven by the Jahn-Teller distortion of Nb_4S_4 molecular clusters. In addition, we also found evidence for a dynamic Jahn-Teller effect preceding the long-range orbital ordering. In contrast to its ferroelectric sister compounds, $GaNb_4S_8$ is the first example indicating that cluster Jahn-Teller effect can also provide a noncanonical mechanism for the emergence of antiferroelectricity.

This work was supported by the Deutsche Forschungsgemeinschaft through the Transregional Collaborative Research Center TRR 80 and via the research project Grant No. KE 2370/3-1. We also acknowledge the support by the Project No. ANCD 20.80009.5007.19 (Moldova). L. P. acknowledges support of Deutscher Akademischer Austauschdienst (DAAD).

[1] C. G. Shull and J. S. Smart, Detection of antiferromagnetism by neutron diffraction, Phys. Rev. **76**, 1256 (1949).
[2] P. Wadley, B. Howells, J. Železný, C. Andrews, V. Hills, R. P. Campion, V. Novák, K. Olejník, F. Maccherozzi, S. S. Dhesi, S. Y. Martin *et al.*, Electrical switching of an antiferromagnet, Science **351**, 587 (2016).
[3] T. Jungwirth, X. Marti, P. Wadley, and J. Wunderlich, Antiferromagnetic spintronics, Nat. Nanotechnol. **11**, 231 (2016).
[4] T. Jungwirth, J. Sinova, A. Manchon, X. Marti, J. Wunderlich, and C. Felser, The multiple directions of antiferromagnetic spintronics, Nat. Phys. **14**, 200 (2018).
[5] R. Lebrun, A. Ross, S. A. Bender, A. Qaiumzadeh, L. Baldrati, J. Cramer, A. Brataas, R. A. Duine, and M. Kläui, Tunable long-distance spin transport in a crystalline antiferromagnetic iron oxide, Nature (London) **561**, 222 (2018).
[6] X. Hao, J. Zhai, L. B. Kong, and Z. Xu, A comprehensive review on the progress of lead zirconate-based antiferroelectric materials, Prog. Mater. Sci. **63**, 1 (2014).
[7] H. Liu and B. Dkhil, A brief review on the model antiferroelectric $PbZrO_3$ perovskite-like material, Z. Kristallogr. Crys. Mater. **226**, 163 (2011).
[8] J. Hlinka, T. Ostapchuk, E. Buixaderas, C. Kadlec, P. Kuzel, I. Gregora, J. Kroupa, M. Savinov, A. Klic, J. Drahokoupil *et al.*, Multiple Soft-Mode Vibrations of Lead Zirconate, Phys. Rev. Lett. **112**, 197601 (2014).
[9] A. K. Tagantsev, K. Vaideeswaran, S. B. Vakhrushev, A. V. Filimonov, R. G. Burkovsky, A. Shaganov, D. Andronikova, A. I. Rudskoy, A. Q. R. Baron *et al.*, The origin of antiferroelectricity in $PbZrO_3$, Nat. Commun. **4**, 2229 (2013).
[10] P. Tolédano and D. D. Khalyavin, Symmetry-determined antiferroelectricity in $PbZrO_3$, $NaNbO_3$, and $PbHfO_3$, Phys. Rev. B **99**, 024105 (2019).
[11] H. Takezoe, E. Gorecka, and M. Čepič, Antiferroelectric liquid crystals: Interplay of simplicity and complexity, Rev. Mod. Phys. **82**, 897 (2010).
[12] R. W. Smith, C. Hu, J. Liu, W.-N. Mei, and K.-J. Lin, Structure and antiferroelectric properties of cesium niobate, $Cs_2Nb_4O_11$, J. Solid State Chem. **180**, 1193 (2007).
[13] H. Unoki and T. Sakudo, Dielectric Anomaly and Improper Antiferroelectricity at the Jahn-Teller Transitions in Rare-Earth Vanadates, Phys. Rev. Lett. **38**, 137 (1977).
[14] K. Kishimoto, T. Ishikura, H. Nakamura, Y. Wakabayashi, and T. Kimura, Antiferroelectric lattice distortion induced by ferroquadrupolar order in $DyVO_4$, Phys. Rev. B **82**, 012103 (2010).

[15] J. Albers, A. Klöpperpieper, H. Rother, and K. Ehses, Antiferroelectricity in betaine phosphate, Phys. Status Solidi A **74**, 553 (1982).

[16] S. Horiuchi, R. Kumai, and S. Ishibashi, Strong polarization switching with low-energy loss in hydrogen-bonded organic antiferroelectrics, Chem. Sci. **9**, 425 (2018).

[17] H. C. Wu, J. K. Yuan, K. D. Chandrasekhar, C. H. Lee, W. H. Li, C. W. Wang, J. M. Chen, J.-Y. Lin, H. Berger, T. W. Yen *et al.*, Observation of charge-transfer driven antiferroelectricity in 3d-pyrochlore multiferroic Cu_2OCl_2, Mater. Today Phys. **8**, 34 (2019).

[18] C. Milesi-Brault, C. Toulouse, E. Constable, H. Aramberri, V. Simonet, S. de Brion, H. Berger, L. Paolasini, A. Bosak, J. Íñiguez *et al.*, Archetypal Soft-Mode-Driven Antipolar Transition in Francisite $Cu_3Bi(SeO_3)_2O_2Cl$, Phys. Rev. Lett. **124**, 097603 (2020).

[19] K. M. Rabe, Antiferroelectricity in oxides: A reexamination, in *Functional Metal Oxides* (John Wiley & Sons, New York, 2013), Chap. 7, p. 221.

[20] P. Tolédano and M. Guennou, Theory of antiferroelectric phase transitions, Phys. Rev. B **94**, 014107 (2016).

[21] S. V. Streltsov and D. I. Khomskii, Orbital physics in transition metal compounds: New trends, Phys. Usp. **60**, 1121 (2017).

[22] S. Reschke, F. Meggle, F. Mayr, V. Tsurkan, L. Prodan, H. Nakamura, J. Deisenhofer, C. A. Kuntscher, and I. Kézsmárki, Lattice dynamics and electronic excitations in a large family of lacunar spinels with a breathing pyrochlore lattice structure, Phys. Rev. B **101**, 075118 (2020).

[23] H.-S. Kim, K. Haule, and D. Vanderbilt, Molecular Mott state in the deficient spinel GaV_4S_8, Phys. Rev. B **102**, 081105(R) (2020).

[24] H. Barz, New ferromagnetic molybdenum spinels, Mater. Res. Bull. **8**, 983 (1973).

[25] H. Ben Yaich, J. C. Jegaden, M. Potel, M. Sergent, A. K. Rastogi, and R. Tournier, Nouveaux chalcogénures et chalcohalogénures á clusters tétraédriques Nb_4 ou Ta_4, J. Less Common Met. **102**, 9 (1984).

[26] D. Johrendt, Crystal and electronic structure of the tetrahedral V_4 cluster compounds GeV_4Q_8 (Q = S, Se), Z. Anorg. Allg. Chem. **624**, 952 (1998).

[27] R. Pocha, D. Johrendt, B. Ni, and M. M. Abd-Elmeguid, Crystal structures, electronic properties, and pressure-induced superconductivity of the tetrahedral cluster compounds $GaNb_4S_8$, $GaNb_4Se_8$, and $GaTa_4Se_8$, J. Am. Chem. Soc. **127**, 8732 (2005).

[28] R. Pocha, D. Johrendt, and R. Pöttgen, Electronic and structural instabilities in GaV_4S_8 and $GaMo_4S_8$, Chem. Mater. **12**, 2882 (2000).

[29] E. Ruff, S. Widmann, P. Lunkenheimer, V. Tsurkan, S. Bordács, I. Kézsmárki, and A. Loidl, Multiferroicity and skyrmions carrying electric polarization in GaV_4S_8, Sci. Adv. **1**, e1500916 (2015).

[30] E. Ruff, A. Butykai, K. Geirhos, S. Widmann, V. Tsurkan, E. Stefanet, I. Kézsmárki, A. Loidl, and P. Lunkenheimer, Polar and magnetic order in GaV_4Se_8, Phys. Rev. B. **96**, 165119 (2017).

[31] E. Neuber, P. Milde, Á. Butykai, S. Bordács, H. Nakamura, T. Waki, Y. Tabata, K. Geirhos, P. Lunkenheimer, and I. Kézsmárki, Architecture of nanoscale ferroelectric domains in $GaMo_4S_8$, J. Phys. Condens. Matter **30**, 445402 (2018).

[32] K. Geirhos, S. Krohns, H. Nakamura, T. Waki, Y. Tabata, I. Kézsmárki, and P. Lunkenheimer, Orbital-order driven ferroelectricity and dipolar relaxation dynamics in multiferroic $GaMo_4S_8$, Phys. Rev. B **98**, 224306 (2018).

[33] Ke Xu and H. J. Xiang, Unusual ferroelectricity induced by the Jahn-Teller effect: A case study on lacunar spinel compounds, Phys. Rev. B **92**, 121112(R) (2015).

[34] P. Barone, K. Yamauchi, and S. Picozzi, Jahn-Teller distortions as a novel source of multiferroicity, Phys. Rev. B **92**, 014116 (2015).

[35] Zhe Wang, E. Ruff, M. Schmidt, V. Tsurkan, I. Kézsmárki, P. Lunkenheimer, and A. Loidl, Polar Dynamics at the Jahn-Teller Transition in Ferroelectric GaV_4S_8, Phys. Rev. Lett. **115**, 207601 (2015).

[36] S. Ghara, K. Geirhos, L. Kuerten, P. Lunkenheimer, V. Tsurkan, M. Fiebig, and I. Kézsmárki, Giant conductivity of non-oxide domain walls (unpublished).

[37] K. Geirhos, B. Gross, B. G. Szigeti, A. Mehlin, S. Philipp, J. S. White, R. Cubitt, S. Widmann, S. Ghara, P. Lunkenheimer *et al.*, Macroscopic manifestation of domain-wall magnetism and magnetoelectric effect in a Néel-type skyrmion host, npj Quantum Mater. **5**, 44 (2020).

[38] E. Janod, E. Dorolti, B. Corraze, V. Guiot, S. Salmon, V. Pop, F. Christien, and L. Cario, Negative colossal magnetoresistance driven by carrier type in the ferromagnetic Mott insulator GaV_4S_8, Chem. Mater. **27**, 4398 (2015).

[39] I. Kézsmárki, S. Bordács, P. Milde, E. Neuber, L. M. Eng, J. S. White, H. M. Rønnow, C. D. Dewhurst, M. Mochizuki, K. Yanai *et al.*, Néel-type skyrmion lattice with confined orientation in the polar magnetic semiconductor GaV_4S_8, Nat. Mater. **14**, 1116 (2015).

[40] Y. Fujima, N. Abe, Y. Tokunaga, and T. Arima, Thermodynamically stable skyrmion lattice at low temperatures in a bulk crystal of lacunar spinel GaV_4Se_8, Phys. Rev. B **95**, 180410(R) (2017).

[41] S. Bordács, Á. Butykai, B. G. Szigeti, J. S. White, R. Cubitt, A. O. Leonov, S. Widmann, D. Ehlers, H.-A. Krug von Nidda, V. Tsurkan *et al.*, Equilibrium skyrmion lattice ground state in a polar easy-plane magnet, Sci. Rep. **7**, 7584 (2017).

[42] H. M. Zhang, J. Chen, P. Barone, K. Yamauchi, S. Dong, and S. Picozzi, Possible emergence of a skyrmion phase in ferroelectric $GaMo_4S_8$, Phys. Rev. B **99**, 214427 (2019).

[43] S. Jakob, H. Müller, D. Johrendt, S. Altmannshofer, W. Scherer, S. Rayaprol, and R. Pöttgen, Structural and magnetic transitions in the Mott insulator $GaNb_4S_8$, J. Mater. Chem. **17**, 3833 (2007).

[44] See Supplemental Material at http://link.aps.org/supplemental/10.1103/PhysRevLett.126.187601 for experimental details, details on the distortion mode analysis, extended and additional reciprocal-space planes, temperature dependence of lattice parameters and cell volume, and details on the weak polarization, which includes Refs. [29,31,43,45–62].

[45] A. Reisinger, N. Trapp, I. Krossing, S. Altmannshofer, V. Herz, M. Presnitz, and W. Scherer, Homoleptic silver (i) acetylene complexes, Angew. Chem. Int. Ed. **46**, 8295 (2007).

[46] J. Langmann, A. Fischer, and G. Eickerling, *Htd2Predict* (University of Augsburg, Augsburg, Germany, 2019).
[47] A. J. M. Duisenberg, Indexing in single-crystal diffractometry with an obstinate list of reflections, J. Appl. Crystallogr. **25**, 92 (1992).
[48] A. J. M. Duisenberg, L. M. J. Kroon-Batenburg, and A. M. M. Schreurs, An intensity evaluation method: *EVAL*-14, J. Appl. Crystallogr. **36**, 220 (2003).
[49] F. Fauth, I. Peral, C. Popescu, and M. Knapp, The new material science powder diffraction beamline at ALBA synchrotron, Powder Diffr. **28**, S360 (2013).
[50] V. Petříček, M. Dušek, and L. Palatinus, Crystallographic computing system JANA2006: General features, Z. Krist. **229**, 345 (2014).
[51] J. Varignon, N. C. Bristowe, E. Bousquet, and P. Ghosez, Coupling and electrical control of structural, orbital and magnetic orders in perovskites, Sci. Rep. **5**, 15364 (2015).
[52] J. Varignon, M. Bibes, and A. Zunger, Origins versus fingerprints of the Jahn-Teller effect in d-electron abX_3 perovskites, Phys. Rev. Research **1**, 033131 (2019).
[53] H. T. Stokes, D. M. Hatch, B. J. Campbell, and D. E. Tanner, Isodisplace: A web-based tool for exploring structural distortions, J. Appl. Crystallogr. **39**, 607 (2006).
[54] K. Singh, C. Simon, E. Cannuccia, M.-B. Lepetit, B. Corraze, E. Janod, and L. Cario, Orbital-Ordering-Driven Multiferroicity and Magnetoelectric Coupling in GeV_4S_8, Phys. Rev. Lett. **113**, 137602 (2014).
[55] Y. Kohara, Y. Yamasaki, Y. Onose, and Y. Tokura, Excess-electron induced polarization and magnetoelectric effect in yttrium iron garnet, Phys. Rev. B **82**, 104419 (2010).
[56] H. Nhalil, H. S. Nair, C. M. N. Kumar, A. M. Strydom, and S. Elizabeth, Ferromagnetism and the effect of free charge carriers on electric polarization in the double perovskite Y_2NiMnO_6, Phys. Rev. B **92**, 214426 (2015).
[57] X. Dai, J. F. Li, and D. Viehland, Weak ferroelectricity in antiferroelectric lead zirconate, Phys. Rev. B **51**, 2651 (1995).
[58] T. Nagai, H. Shirakuni, A. Nakano, H. Sawa, H. Moriwake, I. Terasaki, and H. Taniguchi, Weak ferroelectricity in $n = 2$ pseudo Ruddlesden-Popper-type niobate $Li_2SrNb_2O_7$, Chem. Mater. **31**, 6257 (2019).
[59] E. Constable, S. Raymond, S. Petit, E. Ressouche, F. Bourdarot, J. Debray, M. Josse, O. Fabelo, H. Berger, S. deBrion *et al.*, Magnetic and dielectric order in the kagome-like francisite $Cu_3Bi(SeO_3)_2O_2Cl$, Phys. Rev. B **96**, 014413 (2017).
[60] X. Wei, A. K. Tagantsev, A. Kvasov, K. Roleder, C. Jia, and N. Setter, Ferroelectric translational antiphase boundaries in nonpolar materials, Nat. Commun. **5**, 3031 (2014).
[61] W. Schranz, I. Rychetsky, and J. Hlinka, Polarity of domain boundaries in nonpolar materials derived from order parameter and layer group symmetry, Phys. Rev. B **100**, 184105 (2019).
[62] P. Lunkenheimer, V. Bobnar, A. V. Pronin, A. I. Ritus, A. A. Volkov, and A. Loidl, Origin of apparent colossal dielectric constants, Phys. Rev. B **66**, 052105 (2002).
[63] P. Lunkenheimer, S. Krohns, S. Riegg, S. G. Ebbinghaus, A. Reller, and A. Loidl, Colossal dielectric constants in transition-metal oxides, Eur. Phys. J. Special Topics **180**, 61 (2009).
[64] T. Waki, Y. Kajinami, Y. Tabata, H. Nakamura, M. Yoshida, M. Takigawa, and I. Watanabe, Spin-singlet state formation in the cluster Mott insulator $GaNb_4S_8$ studied by μSR and NMR spectroscopy, Phys. Rev. B **81**, 020401(R) (2010).
[65] H. Ishikawa, T. Yajima, A. Matsuo, Y. Ihara, and K. Kindo, Nonmagnetic Ground States and a Possible Quadrupolar Phase in $4d$ and $5d$ Lacunar Spinel Selenides GaM_4Se_8 (M = Nb, Ta), Phys. Rev. Lett. **124**, 227202 (2020).
[66] L. E. Cross and B. J. Nicholson, LV. The optical and electrical properties of single crystals of sodium niobate, Philos. Mag. **46**, 453 (1955).
[67] R. Uppuluri, H. Akamatsu, A. S. Gupta, H. Wang, C. M. Brown, K. E. A. Lopez, N. Alem, V. Gopalan, and T. E. Mallouk, Competing polar and antipolar structures in the Ruddlesden-Popper layered perovskite $Li_2SrNb_2O_7$, Chem. Mater. **31**, 4418 (2019).